

# Chandra Observation of the Interaction between the Hot Plasma Nebula RCW89 and the Pulsar Jet of PSR B1509–58

Y. Yatsu<sup>1</sup>, J. Kataoka<sup>1</sup>, N. Kawai<sup>1</sup>, and T. Kotani<sup>1</sup>

*Tokyo Institute of Technology, 2-12-1 Ohokayama, Meguro, Tokyo Japan 152-8551*

yatsu@hp.phys.titech.ac.jp

K. Tamura<sup>2</sup>

*Nagoya University*

and

W. Brinkmann<sup>3</sup>

*Max-Planck-Institut für Extraterrestrische Physik  
Postfach 1603, 85740 Garching, Germany*

## ABSTRACT

We present a *Chandra* observation of the H II region RCW89. The nebula lies on 10' north from the central pulsar PSR B1509–58, and it has been suggested that the nebula is irradiated by the pulsar jet. We performed a spectral analysis of the seven brightest emitting regions aligned in a “horse-shoe” shape, and found that the temperature of the knots increases along the “horse-shoe” in the clockwise direction, while, in contrast, the ionization parameter  $n_e t$  decreases. This strongly supports a picture of energy transfer via the precessing pulsar jet. We examined the energy budget assuming that RCW89 is powered by the pulsar jet, and confirmed that the pulsar rotational energy loss is sufficient to drive the nebula. The rate of energy injection into RCW89 by the jet was estimated from the synchrotron radiation flux. We obtained a heating time-scale of 1400 yr, which is consistent with the pulsar characteristic age of 1700 yr. To explain the temperature gradient, we discuss the cooling process for plasma clouds in RCW89. We argue that the plasma clouds can be cooled down by the adiabatic expansion within 70 yr, and form the temperature gradient reflecting the sequential heating by the precessing pulsar jet. We also determined the velocities of the individual plasma clouds by spectral fitting. The plasma clouds in RCW89 are moving away at  $240 \sim 860 \text{ km s}^{-1}$ , which constrains the inclination angle of the pulsar spin axis  $i > 50^\circ$  and the expanding velocity of the shell as  $v_{\text{shell}} > 1100 \text{ km s}^{-1}$ .

*Subject headings:* pulsars, supernovae, supernova remnants

## 1. Introduction

Recent high-resolution X-ray imaging of young energetic pulsars have revealed the ubiquitous presence of “jets” or collimated outflows along the symmetry axis, as seen in the Crab pulsar (Brinkmann, Aschenbach, and Langmeier, 1985; Hester et al. 1995; Weisskopf et al. 2000), the Vela pulsar (Helfand, Gotthelf, & Halpern 2001; Pavlov et al. 2002), and PSR B1509-58 (Trussoni et al. 1996; Gaensler et al. 2002). These jets are probably formed by the relativistic outflows of pulsar magnetospheres, but their composition, energy contents, collimation mechanism, and their relation to the ring- or disk-like pulsar wind nebulae have not been understood. Investigations of pulsar jets allow us to understand the mechanism of particle acceleration and interaction between the pulsar wind and the interstellar medium. Particularly intriguing is the case with PSR B1509-58, which is accompanied by an unidentified thermal nebula RCW89 on the terminus of the pulsar jet. Because of its location, RCW89 has been considered to be a contact point of the jet and the surrounding SNR or the ambient medium. If it is indeed the case RCW89 could be a precious probe for the mysterious pulsar jet.

The supernova remnant (SNR) G320.4-01.2 (MSH15-52, Kes23) has bilateral radio shells with a diameter of  $\sim 30$  arcmin (Caswell, Milne & Wellington 1981). PSR B1509-58, a 150 ms X-ray, radio, and gamma-ray pulsar, is located at the center of G320.4-01.2 (Seward & Harnden 1982; Manchester, Tuohy, & D’Amico 1982). From the spin parameters, a characteristic age  $\tau_c = 1700$  yr (Kaspi et al. 1993), a spin-down luminosity  $\dot{E} = 1.8 \times 10^{37}$  erg s $^{-1}$ , and a surface magnetic field  $B_p = 1.5 \times 10^{13}$  G have been obtained, making it one of the youngest, the most energetic, and the highest field pulsars ever known. The age of 6–20 kyr for the SNR has been derived by assuming standard parameters for the ISM and for the supernova explosion. But this age is an order of magnitude larger than the characteristic age of the pulsar. Although the SNR has a complex structure with multiple components, H I absorption measurements confirm that it is a single SNR at a distance of  $5.2 \pm 1.4$  kpc (Gaensler et al. 1999), suggesting that both the pulsar and the SNR originate from the same supernova.

The H $\alpha$  emission nebula RCW89 was discovered by Rogers, Campbell, & Whiteoak (1960) and coincides with the brightest portion of G320.4-01.2 in radio. It also coincides with one (north nebula) of the two clearly distinguishable X-ray nebulae observed by the *Einstein* Observatory (Seward et al. 1983). The X-ray images taken by *ROSAT* show the distribution of the plasma clumps into a “horse-shoe” like shape (Trussoni et al. 1996; Brazier et al. 1997). Two possible candidates have been proposed for the energy source of the thermal nebula: the supernova blast wave, and the pulsar jet (Manchester 1987). From the analysis of *ASCA* data, Tamura et al. (1996) found a bridge of non-thermal emission connecting the pulsar to the thermal emission. They also found that in RCW89 region thermal emission with prominent line features is dominant. The analysis of the thermal X-ray spectra showed that its energy content was consistent with being powered by the pulsar through the jet. They also argued that a less collimated jet or the precession of the jet is required for heating the spatially extended plasma.

Gaensler et al. (1999) reported detailed radio observations using the Australia Telescope

Compact Array (ATCA). Due to the correspondence of the radio synchrotron knots with the clumps in the X-ray image, they propose that the pulsar is interacting with RCW89 through the jet, and that the non-thermal knots are embedded in the diffuse nebula emitting the thermal X-rays. This picture was however questioned by the *Chandra* data showing that all the knots in RCW89 have thermal spectra (Gaensler et al.2002). Thus the model involving thermal clumps embedded in a diffuse synchrotron nebula (as proposed by Tamura et al. 1996) seems more likely. In this case the energy budget discussed by Tamura et al. (1996) must be reconsidered; *Chandra* has revealed that the energy content in the knots is by two orders of magnitude smaller than that deduced from the *ASCA* observations.

## 2. Observation and Results

G320.4–01.2 was observed on 2000 August 14 with the Advanced CCD Imaging Spectrometer (ACIS) I-array aboard *Chandra*. The net exposure time was 19039 s after removing small intervals in which no data were recorded (Gaensler et al. 2002). A smoothed X-ray image in the energy range 0.4–8.0 keV is shown in Figure 1.

PSR B1509–58, accompanied by the bright PWN, is at the center of the FOV of the ACIS-I and the jet features are extended toward the north-west and south-east direction. RCW89 lies on the end point of the north-west jet, exhibiting a complicated clumpy structure. We extracted photons from the brightest seven emitting regions (labeled as 1–7 in clockwise direction in Fig. 1) and the jet region for comparison, using the *psextract* script of CIAO 2.3 and carried out a spectral analysis. The background was taken from the area marked in Figure 1. Figure 2 shows the spectra of the north jet and region A. The spectrum of the north jet is well fitted by a single power law function with a photon index of  $\Gamma = 2.07 \pm 0.11$  and a hydrogen absorption column density of  $N_H = (0.86 \pm 0.09) \times 10^{22} \text{ cm}^{-2}$  with a  $\chi^2_{\text{red}} = 0.981$  for 70 d.o.f.. The absorption corrected flux density for the energy range 0.5–5.0 keV is  $(1.26 \pm 0.09) \times 10^{-12} \text{ ergs s}^{-1}$ .

The energy spectra of RCW89 regions are quite complex and show strong emission lines as well as a hard high energy tail, which has already been found in the *ASCA* data (Tamura et al 1996). For the analysis of individual knots in RCW89, the photon statistics was not sufficient to determine the column density  $N_H$  and the photon index  $\Gamma$  for each knot independently. To determine the spectral parameters for each knot we first analyzed the spectrum of the total region A in Figure 1, which contains all of the bright knots 2–7. The spectrum of the region “A” is shown in Figure 2. We applied two component model consisting of a non-equilibrium ionization model (“VNEI” in XSPEC 11.3.0) for the thermal component and a power law for the high energy tail. In the NEI model, the metal abundances of Ne, Mg, Si, and Fe, which all have remarkable line emission, were set to be variable. The best fit parameters are shown in Table 1. The column density and the photon index were obtained as  $N_H = (1.18 \pm 0.01) \times 10^{22} \text{ cm}^{-2}$  and  $\Gamma = 2.48 \pm 0.05$  with a  $\chi^2_{\text{red}} = 1.727$  for 227 d.o.f. The fit is rather poor which is mainly due to large residuals in the energy range of 1.0–1.3 keV. For the individual spectral analysis we used fixed values of

$N_H = 1.18 \times 10^{22} \text{cm}^{-2}$  and  $\Gamma = 2.48$ . The results of the spectral analysis for each knot are shown in Table 2.

Figure 3 shows the temperatures and ionization parameters  $n_e t$  from the individual fits to the knots of RCW89. This allows a crude estimate of the physical age of each cloud. The temperatures tend to increase along the “horse-shoe” in a clockwise direction from knots 1 to 7, while the ionization parameter decreases. This result implies that the knots on the north edge of RCW89 consist of freshly heated hot plasma and are still in the state of non-equilibrium ionization while the clouds in the southern regions are close to ionization equilibrium.

### 3. Discussion

In the previous sections, we show clear evidence for variations of plasma parameters (temperature and age) in bright knots in RCW89. There are two possibilities to account for the thermal X-ray emission from RCW89, (1) shock heating due to the supernova blast wave and (2) heating by the pulsar jet of PSR B1509–58. To constrain the energy source of RCW89, we evaluate the ages of the plasma clouds. The *Chandra* image yields the volumes for emitting plasma clouds, assuming that the shapes of the clouds are ellipsoids with major and minor axes of  $l_a$  and  $l_b$  in arcsec. We obtain the number densities of the electrons in the clouds as

$$n_e = 7.0 \times 10^2 (l_a l_b^2)^{-1/2} \left( \frac{EM}{10^{56} \text{ cm}^{-3}} \right)^{1/2} \left( \frac{d_L}{5.2 \text{ kpc}} \right)^{-1/2} \text{ cm}^{-3}, \quad (1)$$

where  $EM$  is the emission measure for each cloud derived from the spectral fits above. Dividing the ionization parameter  $n_e t$  by the electron number density  $n_e$  provides the ionization age  $t_p$ .

$$t_p = 4.5 \times (l_a l_b^2)^{1/2} \left( \frac{n_e t}{10^{11} \text{ s cm}^{-3}} \right) \left( \frac{EM}{10^{56} \text{ cm}^{-3}} \right)^{-1/2} \left( \frac{d_L}{5.2 \text{ kpc}} \right)^{1/2} \text{ yr}. \quad (2)$$

The resulting ages of the plasma clouds are shown in Table 3. Their ages are in the ranged of 5 ~ 700 yr, which is clearly different from each other. Thus, it is not likely that all the knots of RCW89 were heated simultaneously by the supernova blast-wave.

Next, we examine the second hypothesis (that the knots were heated by the pulsar jet) based on the energy budget of the plasma clouds. The internal thermal energy stored in a plasma cloud is estimated as

$$E_{th} = 6.7 \times 10^{45} (l_a l_b^2)^{1/2} \left( \frac{EM}{10^{56} \text{ cm}^{-3}} \right)^{1/2} \left( \frac{kT}{1 \text{ keV}} \right) \left( \frac{d_L}{5.2 \text{ kpc}} \right)^{5/2} \text{ ergs}, \quad (3)$$

which are shown as  $E_{th}$  in Table 3. The total energy in the seven knots amounts to  $2.6 \times 10^{47} (d_L/5.2 \text{ kpc})^{5/2}$  ergs. The heating time scale can be constrained by taking the observable pulsar jet flow into account. The non-thermal flux in the north jet region represents the synchrotron emission from the relativistic electrons. From the spectral fit in Table 1, we therefore infer that

unabsorbed spectral luminosity at 1 keV is  $L_{1 \text{ keV}} = 2.1 \times 10^{33} \text{ ergs s}^{-1} \text{ keV}^{-1}$  for a distance of  $d_L = 5.2 \text{ kpc}$ . We assume the jet to be a cylinder of length  $l_j = 3 \times 10^{18} \text{ cm}$  and cross section  $S_j = 2.0 \times 10^{35} \text{ cm}^2$ . Assuming equipartition between electrons and magnetic field, we obtain the minimum energy of electrons and magnetic field in the jet,

$$E_{jet} = 6.4 \times 10^{35} (1 + \mu)^{4/7} f^{3/7} (\cos i)^{-3/7} \text{ ergs}, \quad (4)$$

where  $f$  is the filling factor, and  $\mu$  is the ratio of ion to electron energy.  $i$  is the inclination angle of the jet. The obtained energy  $E_{jet}$  corresponds to a magnetic field  $B_{jet} \sim 34 \mu\text{G}$  in the north jet, which is consistent with  $B \sim 25 \mu\text{G}$  in the south jet evaluated by Gaensler et al. (2002). The observed photon index for the north jet is  $\sim 2.0$ , while the south jet in the vicinity of the pulsar has a photon index of 1.6. This result implies that the synchrotron electrons emitting in the observed energy band had been cooled before the jet reached the terminal. In a magnetic field  $B \sim 34 \mu\text{G}$ , the life time of synchrotron electrons which emit 1 keV photons is  $\sim 50 \text{ yr}$ . Assuming that the electrons are accelerated in the vicinity of the pulsar, the life time of the electron constrain the velocity of the north jet,

$$v_{jet} \leq 0.5c \left( \frac{l}{7.5 \text{ pc}} \right) \left( \frac{t_{cool}}{50 \text{ yr}} \right)^{-1} \quad (5)$$

where  $l$  is the distance between the “jet (north)” region marked in Figure 1 and the central pulsar.

For a bulk velocity of the jet  $v_{\text{BLK}} \sim 0.5c$ , analogous to that of the Crab nebula (Hester et al. 2002), the power injected into RCW89 amounts to

$$\dot{E}_{jet} = 3.2 \times 10^{35} (1 + \mu)^{4/7} f^{3/7} (\cos i)^{4/7} \left( \frac{v_{\text{BLK}}}{0.5c} \right) \text{ ergs s}^{-1}. \quad (6)$$

This corresponds to 1.7% of the pulsar’s total spin-down luminosity. If the ratio at which the pulsar supplies energy to the north jet had not changed, we can evaluate the initial rotation period as 35 ms for a pulsar’s moment of inertia  $10^{45} \text{ g cm}^2$ . With a constant braking index of  $n = 2.8$ , a pulse period of  $P = 150 \text{ msec}$ , and its first derivative  $\dot{P} = 1.5 \times 10^{-12} \text{ s s}^{-1}$  (Kaspi et al. 1993), the required time to heat RCW89 is then 1400 yr. The ages of oldest plasma estimated from the ionization time scale and the heating time scale required by the energy budget are both of the order of  $\sim 10^3 \text{ yr}$ , in a good agreement with the pulsar’s characteristic age of 1700 yr. Thus our results favors the scenario of heating by the pulsar jet rather than the simultaneous shock heating by the blast wave.

With the obtained magnetic field, we can also estimate the luminosity in TeV range. In the magnetic field of  $34 \mu\text{G}$ , the Lorentz factor of the electrons which emit synchrotron photons at 1 keV is  $\sim 2.3 \times 10^8$ . Such ultra-relativistic electrons can up scatter CMB photons up to  $\sim 1 \text{ TeV}$  gamma-ray. The ratio of the inverse Compton luminosity to the synchrotron luminosity can be described as  $L_{IC}/L_{sync} \approx u_{\text{CMB}}/u_{\text{mag}}$ , where  $u_{\text{CMB}}$  and  $u_{\text{mag}}$  are the energy densities of the cosmic microwave background and that of the magnetic field, respectively. Here, we must compare the synchrotron/inverse Compton luminosity correspond to the same population of relativistic electrons. The observed synchrotron luminosity in 0.5-5.0 keV is  $L_{sync} \sim 4.0 \times 10^{33} \text{ ergs s}^{-1}$ . We

infer a luminosity of the inverse Compton component in the north jet  $L_{IC} \sim 3.0 \times 10^{31}$  ergs  $s^{-1}$  in 1.3-13 TeV which corresponds to the energy of CMB photons scattered by the synchrotron electrons emitting in 0.5-5.0 keV. Since the expected energy flux of  $1.0 \times 10^{-15}$  ergs  $s^{-1}$   $cm^{-2}$  is lower than the detection limit of *HESS*, we cannot expect to detect the TeV gamma-rays from the north jet.

The observed temperature of the elder plasma clouds are cooler. This result implies that an effective cooling process was working and have formed the observed temperature gradient. To investigate how the temperature gradient was formed we consider the cooling process of the plasma clouds.

First we examine the radiative cooling. The dominant emission processes from RCW89 are bremsstrahlung and line emission. However, the radiation fluxes observed by *Chandra* are too small to explain the temperature gradient. We find that the cooling time scale of the knots due to optically thin thermal radiation is longer than  $\sim 4000$  yr which is much longer than the pulsar age, and cannot explain the temperature gradient.

Another plausible process is an adiabatic cooling. We discuss two possible cases of adiabatic expansion. In the first case (“*pure expansion*”), the heated gas volume expands without mixing with the ambient matter. In the second case (“*Sedov*”), the hot gas expands like in the *Sedov* phase of an SNR, where the expanding shock front mixes and heats the ambient matter.

In the “*pure*” adiabatic expansion, the temperature  $T$  and the volume  $V$  follow the relation  $TV^{\gamma-1} = \text{const}$ , ( $\gamma$  is the specific heat ratio;  $\gamma = 5/3$  for a monoatomic gas). We consider, for example, the case of the plasma cloud labeled “7” in Figure 1 with a radius of  $r_0 = 2 \times 10^{17}$  cm and a temperature of  $T_0 = 0.6$  keV. From the  $V - T$  relation, a radius of  $r = 2.8 \sim 10^{17}$  cm is expected when the knot cools down to a temperature of 0.3 keV. Assuming that the expansion velocity equals to the sound velocity in the plasma,  $c_s = \left(\frac{\gamma p}{\rho}\right)^{1/2}$  and the thermal pressure of  $p = 2n_e kT$ , the expansion velocity can be expressed as a function of radius  $r$  as

$$\frac{dr}{dt} = \left(\frac{2\gamma kT_0 r_0^2}{m_p}\right)^{1/2} \frac{1}{r}. \quad (7)$$

Integration yields the time required to expand from  $r_0$  to  $r$  as

$$t = \sqrt{\frac{m_p}{8\gamma kT_0 r_0^2}}(r^2 - r_0^2) \quad (8)$$

From this equation, the cooling time is estimated as  $t_{cool} \sim 70$  yr. In this calculation we have assumed that the density of the plasma cloud is much higher than that of the ambient ISM, which thus does not affect the expansion velocity.

Next, we examine the “*Sedov*” case. The radio observations showed that RCW89 lies on the north shell of the SNR (Gaensler et al. 1999, 2002). Therefore, the jet may heat a small volume of the north shell to form a hot plasma which expands into the ambient matter. In the *Sedov*

model the injected energy  $E_0$  is divided into internal energy and into kinetic energy as

$$E_0 = \frac{4}{3}\pi r^3 \left( \frac{p}{\gamma - 1} + \frac{\rho v^2}{2} \right), \quad (9)$$

where  $p$  is the pressure,  $\rho$  is mass density, and  $v$  is the expansion velocity. We crudely approximate the velocity as  $v \sim c_s$ , which yields

$$v = \left( \frac{15}{28\pi} \right)^{1/2} \left( \frac{E_0}{\rho r^3} \right)^{1/2}, \quad (10)$$

where  $E_0$  is the injected energy. For a radius of  $r = 2 \times 10^{17}$  cm, velocity was estimated to be  $v \sim 400$  km s<sup>-1</sup>. The radius  $r$  can be described as a function of time  $t$  by integrating the velocity

$$r = 1.0 \left( \frac{E_0}{\rho} \right)^{1/5} t^{2/5}. \quad (11)$$

The relation between the temperature  $kT$  and the radius  $r$  is obtained by substituting the equation of the state  $p = 2n_e kT$  into the Eq. (10) as

$$kT = \frac{9}{28\pi} \frac{E_0}{(n_p + n_e)r^3}, \quad (12)$$

where  $k$  is Boltzmann constant and  $n_p$  and  $n_e$  are the number densities of proton and electron, respectively. Then we obtain the time scale to cool from  $kT_0$  to  $kT$  as

$$t_{cool} = \left( \frac{9}{56\pi} \right)^{5/6} m_p^{1/2} \left( \frac{E_0}{n_e} \right)^{1/3} \left[ \left( \frac{1}{kT} \right)^{5/6} - \left( \frac{1}{kT_0} \right)^{5/6} \right]. \quad (13)$$

For knot-7 ( $r_0 = 2 \times 10^{17}$  cm,  $T \sim 0.6$  keV,  $n_e = 130\text{cm}^{-3}$ ) the initially injected energy was estimated as  $E_0 \sim 1.3 \times 10^{46}$  ergs. The time required to cool from 0.6 keV to 0.3 keV is about  $\sim 40$  years.

Both the “*pure* expansion” and “*Sedov* model” can provide sufficient cooling to form the temperature gradient within a heating time scale. At this moment it is hard to say which process is more appropriate since we do not understand well enough the environment surrounding the plasma clouds. Moreover, the knots are embedded in a diffuse synchrotron emission. It may be therefore possible that these plasma clouds are confined by the ambient magnetic field, and their expansion may not be as free as we have assumed here in the discussion.

The differences in the temperatures and plasma ages of the knots indicate that RCW89 was heated in sequence. If these plasma clouds have been heated by the pulsar jet, the direction of the jet would vary with the period. From the tendency of the temperature and the plasma age, we infer that the interaction point between the jet and the ISM has shifted along the “horse-shoe” in clockwise direction. This implies the “precession like” motion of the jet. Preceding discussions

about the energy budget and the cooling process indicate that the jet has made only one precession since the birth of the pulsar within a time scale of 1000 yr.

Considering the origin of the matter which forms the hot clouds, the abundance of elements may provide a precious clue. From the spectral fitting we have obtained the metal abundances of the knots in RCW89. The observed iron abundances tend to be smaller than the solar abundance, while Ne and Mg are relatively rich as shown in Table 2. This suggests that the plasma in RCW89 may originate from a type-II supernova. If RCW89 consists of the ejecta from the supernova associated with the central pulsar, the ejecta must have traveled at least  $\sim 7.5$  pc from the SNR center. In order to arrive at RCW89 within 1700 yr, the required velocity of the ejecta is more than  $\sim 4000$  km s $^{-1}$ , which is rather fast for the standard ISM condition.

The fits to the thermal emission component of the knots required non-zero velocity of the emitting gas to account for slight shifts of the fitted line centroids. We can constrain the geometry and the velocity of the ejecta (RCW89) using the velocity of the plasma clouds. Figure 4 (left) shows the observed redshift for the each knot. Except for the knot 3 which has the poorest photon statistic, the redshifts lie on a smooth curve from  $0.9 \times 10^{-3}$  to  $2.9 \times 10^{-3}$ , which correspond to the velocities of  $240 \sim 860$  km s $^{-1}$  along the line of sight. Now we can consider the geometry as shown in Figure 4 (right). The SNR system is approaching us at  $\sim 70$  km s $^{-1}$  due to the rotation of the Galaxy. Using the inclination angle  $i$  between the pulsar spin axis and the line of sight and the half cone angle  $a$  of the precession of the jet, the apparent velocity  $v_{\text{app}}$  is described as

$$v_{\text{app max}} = v_{\text{shell}} \cdot \cos(i - a) - 70^\circ \quad (\text{km s}^{-1}), \quad (14)$$

$$v_{\text{app min}} = v_{\text{shell}} \cdot \cos(i + a) - 70^\circ \quad (\text{km s}^{-1}), \quad (15)$$

where  $v_{\text{shell}}$  is the velocity of the shell boarding RCW89. Dividing eq. 14 with eq. 15 to cancel  $v_{\text{shell}}$  yields the relation of  $i$  and  $a$  as.

$$\frac{\cos(i - a)}{\cos(i + a)} = \frac{v_{\text{app max}} + 70^\circ}{v_{\text{app min}} + 70^\circ} \quad (16)$$

The observed X-ray image (Figure 1) indicates that the open angle  $a$  is smaller than  $20^\circ$ . Thus the inclination angle is constrained as  $i > 50^\circ$ , which is consistent with the estimation  $i > 70^\circ$  by Brazier & Becker. (1997). If we know  $i$  and  $a$ , we can calculate the velocity of the shell. Using equation 14 and 15 give

$$v_{\text{shell}} = \frac{v_{\text{app max}} - v_{\text{app min}}}{2 \sin i \sin a}. \quad (17)$$

For the inclination angle  $i > 50^\circ$  ( $a < 20^\circ$ ), the expanding velocity of the shell is obtained as  $v_{\text{shell}} > 1100$  km s $^{-1}$  (For  $v_{\text{shell}} \sim 4000$  km s $^{-1}$ ,  $i \sim 80^\circ$  and  $a \sim 5^\circ$  are required ).

#### 4. Summary

We presented a *Chandra* study of the H II region RCW89. The observed X-ray image (Figure 1) revealed the complicated clump structure distributed along a “horse-shoe” shape. To investigate



each plasma cloud, we selected the 7 brightest knots marked in Figure 1 and performed spectral analysis for each knot individually. In the model fitting we assumed a NEI model and power law function.

The resulting temperature tend to increases along the “horse-shoe” in the clockwise direction, while the ionization time scale  $\tau$  decreases. The gradation of temperature and  $\tau$  indicate that the knots on the north edge of RCW89 are freshly heated hot plasma and are still in the state of non-equilibrium ionization, while the plasma in the south region are older and more close to ionization equilibrium. This new finding is consistent with the picture that RCW89 nebula is heated by the pulsar jet sequentially.

To confirm the hypotheses, we examined the energy budget for RCW89. The observed emission measure and volume yielded stored thermal energy in the knots as  $E_{th} = 2.6 \times 10^{47}$  ergs. On the other hand, the pulsar jet is supplying relativistic electrons and magnetic energy of  $3.2 \times 10^{35}$  ergs  $s^{-1}$  into RCW89 assuming a condition of equipartition and a bulk velocity of the jet of  $v_{BLK} = 0.5c$ . The jet requires  $\sim 1400$  yr to heat the knots, which is consistent with the pulsar characteristic age.

Next we discussed the cooling process to explain the gradation of the temperature. The most plausible process is adiabatic expansion. If the expansion velocity is the sonic velocity in the thermal plasma, it takes  $\sim 70$  yr for cooling down the knot-7 with typical values of internal energy  $E_{th} = 1.3 \times 10^{46}$  ergs and radius of  $r = 2 \times 10^{17}$  cm from 0.6 keV to 0.3 keV. It is sufficient to form the temperature gradient within the pulsar time scale of 1700 yr.

The spectral fitting provides information on the metal abundance of each knot. The Fe-poor spectra indicate that the matter consisting RCW89 originated in a Type-II supernova. It is consistent with the existence of the pulsar.

The obtained redshifts of the each knots vary with their locations. We estimated the geometry of the pulsar and the velocity of the shell of the SNR using the Doppler shifts of the spectra and the X-ray image. With the precession half cone angle of  $a < 20^\circ$ , the inclination angle is constrained as  $i > 50^\circ$ , and the velocity of the shell as  $v_{shell} > 1100$  km  $s^{-1}$ .

## REFERENCES

- Brazier, K. T. S., & Becker, W. 1997, MNRAS, 284, 335
- Brinkmann, W., Aschenbach, B., & Langmeier, A. 1985, Nature, 313, 662
- Caswell, J. L., Milne, D. K., & Wellington, K. J. 1981 MNRAS, 195, 89
- Gaensler, B. M., Arons, J., Kaspi, V. M., Pivovarov, M. J., Kawai, N., & Tamura, K. 2002, ApJ, 569, 878

- Gaensler, B. M., Brazier, K. T. S., Manchester, R. N., Johnston, S., & Green, A. J. 1999, MNRAS, 305, 724
- Gaensler, B. M., Brazier, K. T. S., Manchester, R. N., Johnston, S., & Green, A. J. 1998, MmSAI, 69, 877
- Helfand, D. J., Gotthelf, E. V., & Halpern, J. P. 2001, ApJ, 556, 380
- Hester, J. J. et al. 1995, ApJ, 448, 240
- Hester, J. J. et al. 2002, ApJ, 577, L49
- Kaspi, V. M., et al. 1994, ApJ, 422, L83
- Manchester, R. N., Tuohy, I. R., & D’Amico, N. 1982, ApJ, 262, L31
- Manchester, R. N., 1987, A&A, 171, 205
- Pavlov, G. G., Teter, M. A., Kargaltsev, O., & Sanwal, D. 2002, ApJ, 591, 1157
- Rodgers A. W., Campbell C. T., Whiteoak J.B., 1960 MNRAS, 121, 103
- Sako, T., et al. 2000, ApJ, 537, 422
- Seward, F. D., & Harnden, F. R. Jr., 1982, ApJ, 256, L45
- Tamura, K., Kawai, N., Yoshida, A., & Brinkmann, W. 1996, PASJ, 48, L33
- Trussoni, E., Massaglia, S., Caucino, S., Brinkmann, W., & Aschenbach, B. 1996, A&A, 306, 581
- Weisskopf et al. 2000, ApJ, 536, L81
- Whiteoak, J. B. Z., Green, A. J. 1996, A&AS, 118, 329

Table 1. Spectral fits to region “A” and “jets” in Figure 1.

Parameters	region-A	jet (north)	jet (south)
Column density ( $10^{22}\text{cm}^{-2}$ )	$1.18 \pm 0.01$	$0.86 \pm 0.09$	$1.02 \pm 0.08$
<i>Thermal component</i>			
Temperature (keV)	$0.38 \pm 0.01$		
$n_e t^{\text{a}}$ ( $10^{11} \text{ s cm}^{-3}$ )	$0.71 \pm 0.05$		
$EM^{\text{b}}$ ( $10^{57} \text{ cm}^{-3}$ )	$3.42 \pm 0.03$		
Abundance (solar abundance)			
Ne	$1.00 \pm 0.03$		
Mg	$0.92 \pm 0.02$		
Si	$0.41 \pm 0.04$		
Fe	$0.32 \pm 0.02$		
<i>Non-thermal component</i>			
Photon index	$2.48 \pm 0.05$	$2.07 \pm 0.11$	$1.66 \pm 0.09$
Flux <sub>0.5–5.0keV</sub> ( $10^{-12} \text{ ergs s}^{-1} \text{ cm}^{-2}$ )	$8.67 \pm 0.05$	$1.26 \pm 0.09$	$4.16 \pm 0.26$
$\chi^2_{\nu}$ ( $\nu$ )	1.727 (227)	0.981 (70)	0.493 (172)

Note. — Errors are with  $1 \sigma$  confidence.

<sup>a</sup>Ionization timescale of the non-equilibrium ionization plasma.

<sup>b</sup>Emission measure  $\int n_e n_H dV (d_L/5.2\text{kpc})^2$  ( $d_L$  is the distance to RCW89).

Table 2. Results from spectra fitting

Region <sup>a</sup>	$kT$ (keV)	$n_{et}$ <sup>b</sup> ( $10^{11}\text{cm}^{-3}\text{s}$ )	$EM$ <sup>c</sup> ( $10^{56}\text{cm}^{-3}$ )	$F_{\text{th}}$ <sup>d</sup> ( $\times 10^{-11}$ )	$F_{\text{PL}}$ <sup>d</sup> ( $\times 10^{-13}$ )	Ne	Mg	Abundance Si	Fe	Redshift ( $\times 10^{-3}$ )	$\chi^2_{\nu}$ ( $\nu$ )
1.....	$0.21^{+0.01}_{-0.02}$	> 11(24.2)	$3.94^{+1.17}_{-2.28}$	$1.93^{+1.14}_{-0.57}$	$2.33^{+0.30}_{-0.34}$	$1.64^{+0.24}_{-0.24}$	$2.46^{+0.68}_{-0.36}$	$1.02^{+1.04}_{-1.02}$	< 0.17(0.00)	$0.83^{+0.27}_{-0.19}$	1.387 (39)
2.....	$0.26^{+0.02}_{-0.01}$	> 11(28.8)	$2.30^{+0.64}_{-0.52}$	$1.29^{+0.31}_{-0.20}$	$4.17^{+0.42}_{-0.42}$	$1.94^{+0.22}_{-0.23}$	$2.99^{+0.61}_{-0.30}$	< 0.90(0.40)	$0.62^{+0.12}_{-0.13}$	$2.74^{+0.13}_{-0.81}$	1.150 (62)
3.....	$0.20^{+0.04}_{-0.03}$	$1.46^{+1.59}_{-0.68}$	$11.56^{+9.14}_{-5.47}$	$6.80^{+3.24}_{-1.29}$	$5.33^{+0.41}_{-0.41}$	$0.54^{+0.14}_{-0.15}$	$1.02^{+0.87}_{-0.19}$	$1.16^{+0.53}_{-0.56}$	$0.14^{+0.34}_{-0.13}$	$-2.50^{+3.05}_{-2.62}$	1.083 (50)
4.....	$0.41^{+0.02}_{-0.01}$	$1.07^{+0.16}_{-0.13}$	$1.43^{+0.16}_{-0.04}$	$1.90^{+0.50}_{-0.32}$	$2.01^{+0.34}_{-0.42}$	$1.52^{+0.13}_{-0.14}$	$1.46^{+0.13}_{-0.11}$	$0.35^{+0.13}_{-0.12}$	$0.30^{+0.07}_{-0.06}$	$2.88^{+1.48}_{-0.15}$	1.682 (61)
5.....	$0.40^{+0.01}_{-0.01}$	$0.70^{+0.07}_{-0.05}$	$8.22^{+0.28}_{-0.29}$	$9.89^{+0.53}_{-0.48}$	$3.11^{+0.59}_{-0.59}$	$1.18^{+0.05}_{-0.05}$	$0.93^{+0.04}_{-0.04}$	$0.50^{+0.06}_{-0.04}$	$0.41^{+0.02}_{-0.04}$	$2.18^{+0.24}_{-0.29}$	1.674 (104)
6.....	$0.52^{+0.02}_{-0.02}$	$0.46^{+0.06}_{-0.05}$	$1.17^{+0.06}_{-0.12}$	$2.94^{+0.48}_{-0.38}$	$2.96^{+0.47}_{-0.46}$	$2.16^{+0.15}_{-0.14}$	$1.77^{+0.10}_{-0.11}$	$0.54^{+0.11}_{-0.11}$	$0.44^{+0.07}_{-0.06}$	$0.95^{+0.10}_{-0.21}$	1.528 (77)
7.....	$0.67^{+0.08}_{-0.08}$	$0.23^{+0.08}_{-0.05}$	$0.53^{+0.13}_{-0.14}$	$1.69^{+0.42}_{-0.41}$	$3.45^{+0.64}_{-0.80}$	$2.16^{+0.48}_{-0.29}$	$1.53^{+0.11}_{-0.23}$	$0.38^{+0.22}_{-0.18}$	$0.12^{+0.12}_{-0.07}$	$0.80^{+0.25}_{-0.11}$	1.335 (64)

Note. — Errors are with  $1\sigma$  confidence. The  $1\sigma$  limits (with the best-fit values in the parentheses) are presented where the best-fit parameters are unconstrained.

<sup>a</sup>Regions as marked in Fig. 1.

<sup>b</sup>Ionization timescale for the non-equilibrium ionization plasma.

<sup>c</sup>Emission measure  $\int n_e n_H dV$  ( $d_L/5.2\text{kpc}$ )<sup>2</sup> ( $d_L$  is the distance toward RCW89.)

<sup>d</sup> $F_{\text{th}}$  and  $F_{\text{PL}}$  are the unabsorbed energy flux in 0.5 – 5.0 keV for the thermal component and for the power-law function, respectively. They are expressed in a unit of  $\text{ergs cm}^{-2} \text{s}^{-1}$ .

Table 3. Estimated plasma parameters assuming  $d_L = 5.2$  kpc

Region <sup>a</sup>	$l_a \times l_b$ <sup>b</sup> (arcsec)	$V$ <sup>c</sup> ( $\text{cm}^3$ )	$n_e$ ( $f^{-1/2} \text{ cm}^{-3}$ )	$E_{\text{thermal}}$ <sup>d</sup> ( $f^{1/2} \text{ ergs}$ )	$t_{\text{plasma}}$ <sup>e</sup> ( $f^{1/2} \text{ yr}$ )
1.....	$2.0 \times 1.7$ $1.5 \times 1.0$	$1.5 \times 10^{52}$	$510_{-180}^{+70}$	$7.7_{-3.2}^{+1.5} \times 10^{45}$	$> 59(150)$
2.....	$8.0 \times 2.5$ $2.0 \times 2.0$	$1.2 \times 10^{53}$	$140_{-20}^{+20}$	$2.1_{-0.3}^{+0.4} \times 10^{46}$	$> 220(660)$
3.....	$2.2 \times 2.0$ $2.7 \times 2.7$	$5.7 \times 10^{52}$	$450_{-120}^{+150}$	$2.5_{-0.9}^{+1.5} \times 10^{46}$	$10_{-6}^{+20}$
4.....	$5.0 \times 2.4$	$5.8 \times 10^{52}$	$160_{-3}^{+9}$	$1.8_{-0.1}^{+0.2} \times 10^{46}$	$22_{-4}^{+4}$
5.....	$15.7 \times 4.9$	$7.5 \times 10^{53}$	$100_{-2}^{+2}$	$1.5_{-0.6}^{+0.6} \times 10^{47}$	$21_{-2}^{+3}$
6.....	$3.4 \times 2.0$ $11.3 \times 2.7$ $1.7 \times 1.7$	$2.0 \times 10^{53}$	$76_{-4}^{+2}$	$3.8_{-0.3}^{+0.2} \times 10^{46}$	$19_{-2}^{+4}$
7.....	$3.8 \times 2.0$	$3.0 \times 10^{52}$	$130_{-18}^{+15}$	$1.3_{-0.3}^{+0.3} \times 10^{46}$	$5_{-2}^{+3}$

Note. — Uncertainties are all at  $1 \sigma$  confidence. The  $1 \sigma$  limits (with the best values in the parentheses) are presented where the best-fit parameters are unconstrained. There still remains uncertainty  $f$ , which is the filling factor or the uncertainty of the emitting volume.

<sup>a</sup>Regions as marked in Fig. 1

<sup>b</sup>Size of the plasma cloud. The axis length ( $2l_a, 2l_b$ ) are defined as the FWHM of the surface brightness. For the region 1, 2, 3, and 6, we measured the size of each distinctive cloud.

<sup>c</sup>Total volume of the plasma clouds in the region.

<sup>d</sup>Internal thermal energy contained in the knots.

<sup>e</sup>Plasma age obtained from the ionization parameter and electron number density ( $n_e t / n_e$ ).

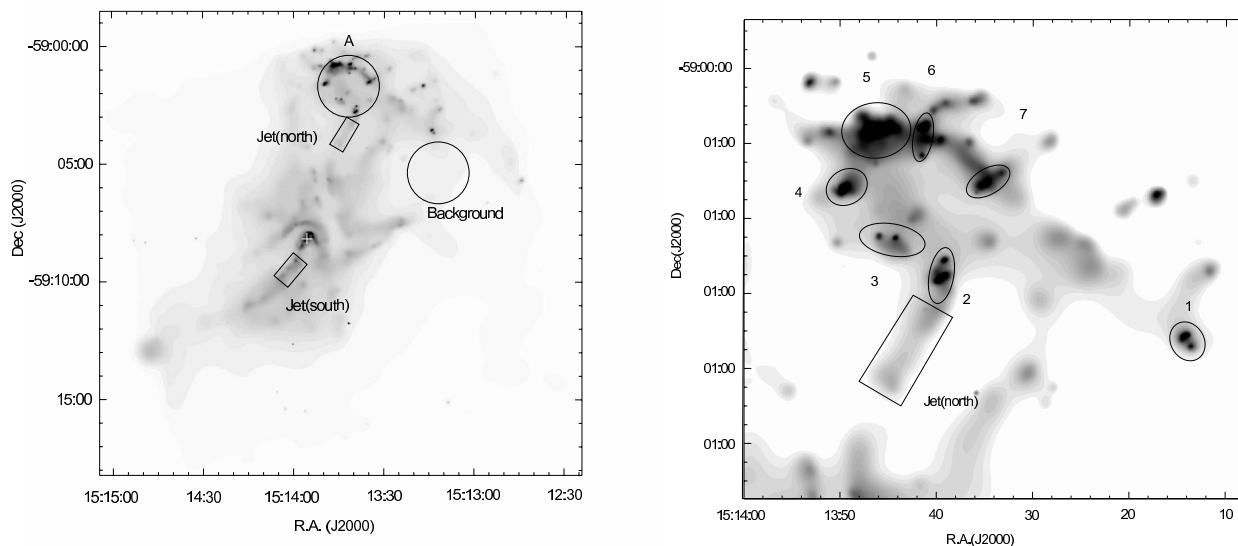


Fig. 1.— (left) An overall X-ray image of RCW89 and PSR B1509–58 in the energy range 0.4–8.0 keV. The pulsar position is marked with a plus sign. (right) A zoom up of the interacting region in RCW89. The ellipses and rectangular regions were selected for succeeding spectral analysis.

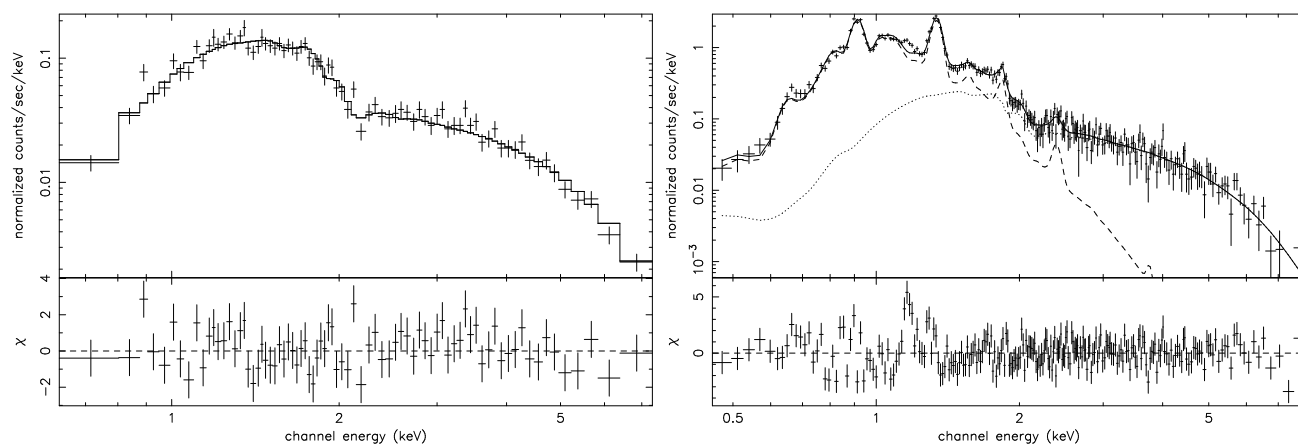


Fig. 2.— Left: Power law fit to the jet region (labeled in Fig. 1) — Right: Model fit to the brightest region in RCW89 labeled “A” in Fig. 1. We used a non-equilibrium ionization model, “VNEI” in XSPEC, for the softer thermal component (dashed line) and a power law model for the hard component (dotted line).

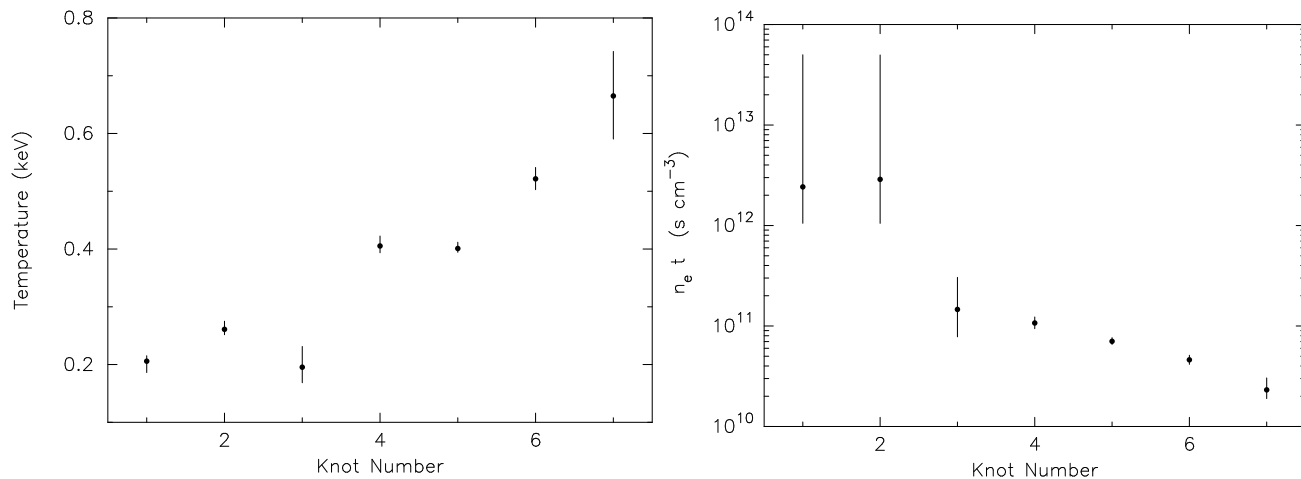


Fig. 3.— Spatial distribution of the temperature (Left) and the ionization time scale  $n_e t$  cm<sup>-3</sup>s (Right). The plasma temperature increases along the “horse-shoe” in clockwise direction, while in contrast,  $n_e t$  decreases. Uncertainties are at 1  $\sigma$  confidence.

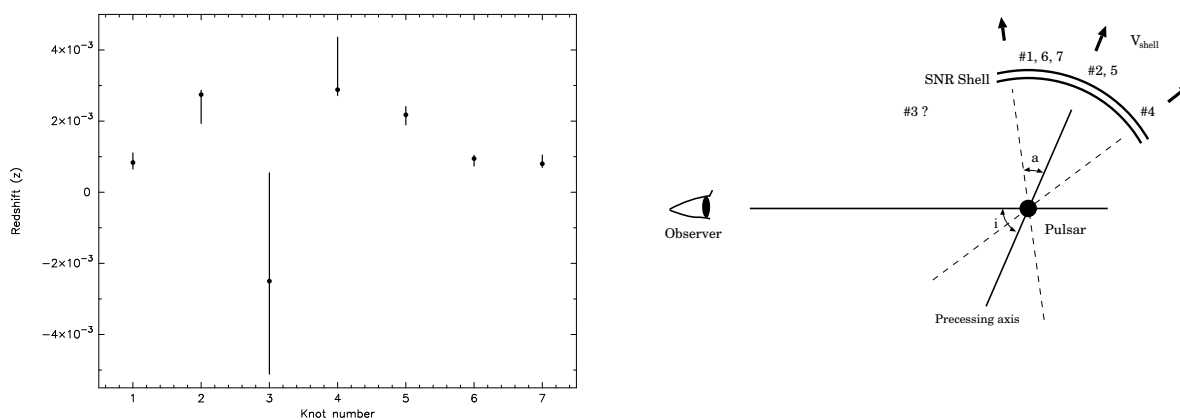


Fig. 4.— Left — The observed redshift for the each plasma cloud. Right — The schematic image of the geometry of the pulsar and RCW89. The errors are 1  $\sigma$ .